JACS
JOURNAL OF THE AMERICAN CHEMICAL SOCIETY

COMMUNICATION

pubs.acs.org/JACS

Rational Solution Growth of α-FeOOH Nanowires Driven by Screw Dislocations and Their Conversion to α-Fe_2O_3 Nanowires

Fei Meng, Stephen A. Morin, and Song Jin*

Department of Chemistry, University of Wisconsin—Madison, 1101 University Avenue, Madison, Wisconsin 53706, United States

Supporting Information

ABSTRACT: We report the rational synthesis of α-FeOOH (goethite) nanowires following a dislocation-driven mechanism by utilizing a continuous-flow reactor and chemical equilibria to maintain constant low supersaturations. The existence of axial screw dislocations and the associated Eshelby twist in the nanowire product were confirmed using bright-/dark-field transmission electron microscopy imaging and twist contour analysis. The α-FeOOH nanowires can be readily converted into semiconducting single-crystal but porous α-Fe_2O_3 (hematite) nanowires via topotactic transformation. Our results indicate that, with proper experimental design, many more useful materials can be grown in one-dimensional morphologies in aqueous solutions via the dislocation-driven mechanism.

Nanowire (NW) growth can be driven by axial screw dislocations which provide self-perpetuating step edges at the tip of NW and break the symmetry of crystal growth.[1] Only two conditions are required to promote dislocation-driven growth: the presence of dislocation sources and low precursor supersaturation.[1d] Distinctly different from the prevailing vapor—liquid—solid or related catalyst-driven mechanisms,[2] dislocation-driven NW growth does not rely on catalysts, and thus the consideration of catalysts/NWs eutectic behaviors, and can be easily conducted in low-temperature aqueous solutions. Therefore, this approach could eventually become more versatile.[1f] Besides the examples of vapor-phase growth of PbS[1a,b] and PbSe[3] pine tree NWs and the solution growth of ZnO NWs and nanotubes (NTs),[1c,d] dislocation-driven growth of $Co(OH)_2$ NWs from solution[4] and strong evidence for dislocation-driven GaN NWs grown via chemical vapor deposition[5] have recently been reported. In particular, by considering fundamental crystal growth theories, the improved synthesis of ZnO NWs illustrates a general framework for rational implementation of dislocation-driven NW growth[1c] that can enable large-scale, low-cost NW synthesis of various functional nanomaterials for diverse applications.[1f] Here we expand such rational synthetic design to a new type of material, Fe(III) oxides/oxyhydroxides NWs, and confirm that their growth is indeed driven by screw dislocations.

Hematite (α-Fe_2O_3, also known as rust) is actually a semiconductor with a bandgap of about 2.1 eV. It is a promising material for solar energy conversion, particularly photocatalysis, due to its stability in aqueous environments.[6] However, its poor semiconducting properties, such as low mobility and short carrier diffusion length, have prevented the bulk material from being used for meaningful applications. Making α-Fe_2O_3 nanoscale, including NWs, can help to circumvent some of these shortcomings by minimizing the distance the minority carriers have to diffuse. Illustrated by recent research efforts toward nanoscale hematite for solar energy conversion, this strategy does yield promising performance characteristics.[7] The family of Fe(III) oxides/oxyhydroxides represents inexpensive, abundant, and stable materials for solar energy conversion applications and perhaps best epitomizes the key advantages of dislocation-driven NW growth.

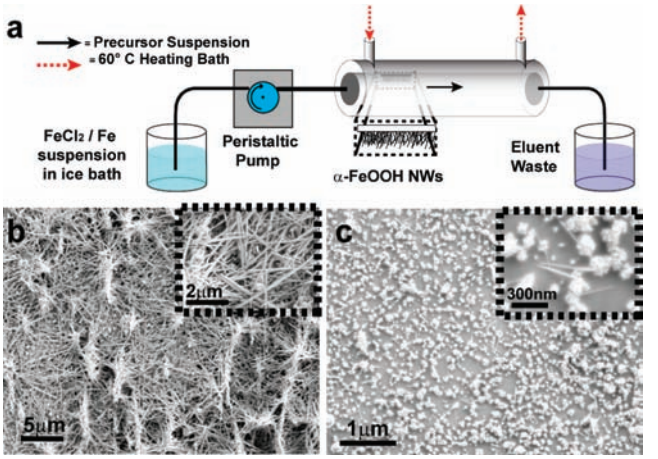

Figure 1. (a) Schematic of the CFR for α-FeOOH NW growth. (b,c) SEM images of α-FeOOH NWs yielded from a CFR reaction (b) and a static hydrothermal reaction (c).

We have designed and accomplished the growth of α-FeOOH NWs with high quality and yield using a continuous-flow reactor (CFR, Figure 1a).[1c] Previous reports on the "spontaneous" catalyst-free growth of Fe(III) oxides/oxyhydroxides one-dimensional (1D) nanostructures invariably employed a forced hydrolysis method in static hydrothermal reactions, sometimes assisted by surfactants or organic ligands[8] but never with intentional supersaturation control. Due to the often lower concentration used and the earlier observations of hollow NTs (a sign of dislocation-driven growth) reported,[8a,b] we hypothesized that their growth was actually driven by screw dislocations and set out to rationally design a well-controlled hydrolysis of low-concentration Fe ions from aqueous solutions to enable the formation of higher quality NWs via the dislocation-driven mechanism. Following classical crystal growth theory,[9] supersaturation (σ),

Received: January 27, 2011
Published: May 11, 2011

dx.doi.org/10.1021/ja200841e | J. Am. Chem. Soc. 2011, 133, 8408–8411

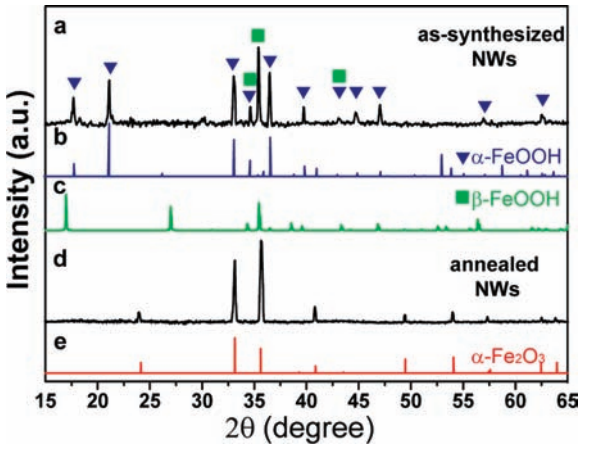

Figure 2. PXRD of as-synthesized (a) and annealed (d) NW samples in comparison with the reference diffractograms for α-FeOOH (b), β-FeOOH (c), and α-Fe_2O_3 (e).

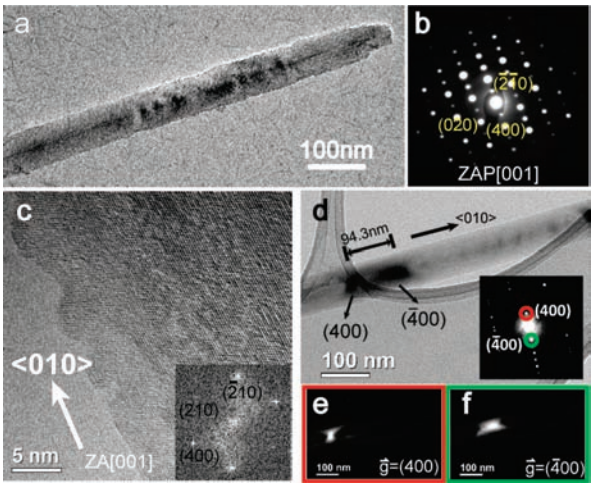

Figure 3. TEM characterization of α-FeOOH NWs. (a) Low-resolution bright-field TEM image of a single NW, revealing the dislocation contrast at the center of the NW. (b) Indexed SAED pattern corresponding to (a). (c) HRTEM image of a single NW, confirming growth along the ⟨010⟩ direction (inset is the corresponding indexed fast Fourier transform). (d) Zero beam bright-field TEM image of a representative NW, showing two indexed twist contours (inset is the SAED pattern). (e,f) Displaced-aperture dark-field TEM used to index the two labeled contours.

defined as $\sigma = \ln(c/c_o)$, where c is the precursor concentration and c_o is the equilibrium concentration, determines the mode of crystal growth. Dislocation growth, layer-by-layer growth, and dendritic growth progressively dominate crystal growth as σ is increased. Therefore, to control the mechanism of crystal growth, it is essential to manipulate the supersaturation of the precursors. However, commonly applied static hydrothermal reactions fail to maintain the precursors' supersaturation, as they are gradually depleted during the reaction, leading to convoluted and poorly controlled growth. The CFR utilized here maintains constant low supersaturation and does not suffer from these issues.

We prepared the precursors for the CFR reaction by mixing a 2.5 mM aqueous solution of $FeCl_2$ with 5 g/L of Fe metal particles with sub-10-μm diameters under vigorous magnetic stirring at 0 °C to give a suspension with a pH of ~6. The precursor suspension was then continuously flowed through the CFR at 60 °C for 4−24 h as Fe ions steadily hydrolyzed to form Fe(III) oxyhydroxides/hydroxides/oxides. A piece of Si or glass substrate was mounted in the CFR to collect the produced NWs. The contrast between the product morphologies seen for a CFR reaction and a static hydrothermal reaction with comparable conditions (see Supporting Information for experimental details) is rather dramatic: there are copious amounts of fairly uniform NWs (Figure 1b) for the CFR reactions, while the static hydrothermal reaction yields mainly microparticles with sparse NW growth (Figure 1c). The NWs are usually 60−80 nm in diameter and vary in length from 2−3 μm to >20 μm, depending on the growth time. In the current case, defective particles are still inevitably produced and likely provide the source of dislocations,[1c] as evidenced by the observation of the seed particles at the end of the NWs (Figure 1c inset).

Powder X-ray diffraction (PXRD, Figure 2a) shows that the majority of the as-synthesized NWs are orthorhombic α-FeOOH (goethite, JCPDS No. 29-0713, space group *Pnma*, a = 9.95 Å, b = 3.01 Å, c = 4.62 Å) with a few impurity peaks that can be attributed to the β-FeOOH (akaganeite, JCPDS No. 34-1266, space group *I*4/*m*, a = 10.44 Å, b = 3.01 Å). Therefore, the hydrolysis reaction taking place is the following:

$$Fe^{3+} + 2H_2O \rightarrow FeOOH + 3H^+$$

We notice that there are a number of reports[8] confirming that the FeOOH phases are the major direct hydrolysis products. The stability of the many different polymorphs of Fe(III) oxides/oxyhydroxides/hydroxides depends on their surface energetics, sizes, and environment. While α-Fe_2O_3 is the most stable phase in bulk, at the nanoscale in a hydrated environment, α-FeOOH is predicted to be the most stable phase due to its much lower surface energy.[10]

In order to guarantee the low supersaturation of Fe^{3+}, which readily hydrolyzes, we have designed two "protection" reactions. First, as mentioned previously, we started with Fe^{2+} ions instead of directly using Fe^{3+} ions. The hydrolysis of Fe^{3+} ions is so favorable [K_{sp} for $Fe(OH)_3 = 4 \times 10^{-38}$] and fast that preventing such favorable hydrolysis (high supersaturation) requires an extremely low pH condition that is inconvenient and unsafe for our current CFR system. On the other hand, Fe^{2+} ions do not hydrolyze and precipitate significantly even at near-neutral pH because the K_{sp} for $Fe(OH)_2$ is 8×10^{-16}, but they can be readily oxidized to Fe^{3+} by the dissolved oxygen in aqueous solution.

$$4Fe^{2+} + O_2 + 4H^+ \rightarrow 4Fe^{3+} + 2H_2O$$

Second, the presence of Fe metal powder further maintains the low supersaturation of Fe^{3+}: Fe would reduce Fe^{3+} back to Fe^{2+} ions and guarantee a constant and low concentration (supersaturation) of Fe^{3+}, as dictated by the Fe^{3+}/Fe^{2+} redox equilibrium.

$$2Fe^{3+} + Fe \rightleftarrows 3Fe^{2+}$$

Transmission electron microscopy (TEM) characterization of the α-FeOOH NWs further confirms the phase identity and that they are indeed dislocation-driven. Select area electron diffraction (SAED) confirms that the NWs are single-crystal α-FeOOH, with the most common zone axes observed being ⟨001⟩ (Figure 3b). We have examined over 30 NW objects using SAED and confirmed that all of these examined NWs are single-

dx.doi.org/10.1021/ja200841e | *J. Am. Chem. Soc.* 2011, 133, 8408–8411

crystal α-FeOOH (Figure S1 in the Supporting Information (SI) shows some of them), so the minor impurity phase seen in the PXRD most likely comes from the occasional microparticles that are still present on the growth substrate. Using high-resolution TEM (HRTEM, Figure 3c), we have determined that the growth directions of these NWs are along ⟨010⟩. A zero beam bright-field TEM image (Figure 3a) of a NW clearly shows a contrast line going through the center of the NW, which is evidence for an axial screw dislocation. Over 15 NWs that contain similar features have been observed (Figure S2, SI), which is approximately half of the total number of the NWs examined. Considering the fact that dislocations in small volumes are especially mobile and that the α-FeOOH is so unstable under high-energy electron beam exposure that sometimes it was converted into α-Fe_2O_3 during observation (Figure S3, SI), such statistics are reasonable.

Further evidence for dislocation-driven growth is the confirmation of Eshelby twist using twist contour analysis. Axial screw dislocations create stress and strain in the NWs, which causes NWs to twist, known as the Eshelby twist,[11] and/or hollow out at the dislocation core, creating tubes.[1c] Interestingly, a few NWs actually have small voids near the dislocation core of the NWs, perhaps indicating the beginning of nanotube formation (Figure S4, SI). Most of our products are solid NWs; therefore, the NWs must be twisting to alleviate the dislocation strain energy. Several methods based on electron microscopy or diffraction techniques have been established to identify the Eshelby twists.[12] Here we quantify the lattice twists using "twist contour" analysis, which involves indexing dark twist contour bands seen along the NWs in zero beam bright-field TEM images, whose principles have been described in our previous work.[1d] To conduct a twist contour analysis, the NW first needs to be oriented in such a way that the **g** vectors that are orthogonal to the NW growth direction are excited. In our case, since the NW growth direction is ⟨010⟩ and the most approachable zone axis is ⟨001⟩, the most probable **g** vectors to excite are from the {100} families (Figure 3d inset). A zero beam bright-field image is then taken to record the locations of the contour bands for measurement of the separation between them. A representative example (Figure 3d) shows a separation of 94.3 nm. To be clear, each twist contour can be uniquely indexed to a certain **g** vector using displaced-aperture dark-field imaging. This is in contrast to bend contours, which can be assigned to multiple **g** vectors. (Some examples are shown in Figure S5, SI.) The two twist contours seen in this example can be indexed to (400) and ($\bar{4}$00) **g** vectors, respectively (Figure 3e,f). The real-space twisting angle (α) is then calculated using the following equation:[1d,12]

$$\alpha = \left(\frac{\lambda}{2L}\right)|\mathbf{g_2} - \mathbf{g_1}|$$

where λ is the wavelength of electrons (2.51 pm here), L is the measured real-space distance between the two indexed twist contours (94.3 nm), and $\mathbf{g_1}$ and $\mathbf{g_2}$ are two opposite reciprocal lattice vectors [(400) and ($\bar{4}$00)]. The calculated twist for the NW shown is 6.1°/μm, which is reasonable for a NW with a diameter of 70 nm. The dislocation contrast observed in TEM together with this twist contour analysis confirms that the NWs grown here follow the screw dislocation-driven mechanism.

The α-FeOOH NWs formed by direct hydrolysis can be readily converted to semiconducting α-Fe_2O_3 NWs by annealing in air from 300 to 600 °C. PXRD confirms that, after the annealing at 600 °C for 8 h, the only crystalline phase present is the hematite, since the α/β-FeOOH peaks completely disappear and the major α-Fe_2O_3 peaks (JCPDS No. 33-06644) emerge (Figure 2d). SAED (Figure 4a inset) also confirms the phase identification of rhombohedral α-Fe_2O_3 (space group $R\bar{3}c$, a = 5.034 Å, c = 13.75 Å) and further shows that the annealed NWs maintain single crystallinity. The thermal dehydration of α-FeOOH NWs to form α-Fe_2O_3 NWs undergoes a topotactic transformation process due to their structural similarity.[13] Interestingly, it seems that the thermal treatment has introduced porosity to α-Fe_2O_3 NWs (Figure 4a,b), which has also been observed in other metal hydroxides/oxides systems.[14] This can be attributed to the loss of water molecules in the lattice that causes an increase in the crystal density [ρ(α-FeOOH) = 4.3 g/cm^3, while ρ(α-Fe_2O_3) = 5.3 g/cm^3]. The porous structure of single-crystal α-Fe_2O_3 NWs could improve the photocatalytic efficiency of water splitting since the small crystal domain size can further decrease the carrier diffusion distance to the electrolytes and increase the surface area.[7]

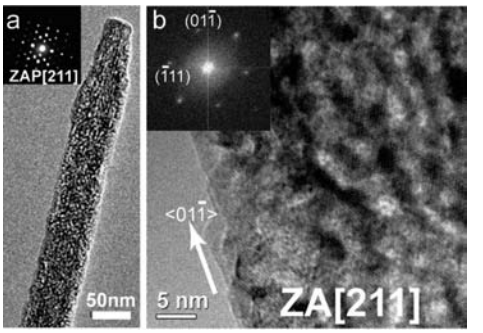

Figure 4. TEM characterization of porous α-Fe_2O_3 NWs annealed at 300 °C for 1 h. (a) Low-resolution bright-field TEM image of a single NW (inset is the corresponding SAED pattern). (b) HRTEM image of a single NW showing ⟨01$\bar{1}$⟩ growth direction and the porous nature (inset is the corresponding indexed fast Fourier transform).

Here we have rationally synthesized α-FeOOH NWs following the dislocation-driven mechanism by using a CFR and other chemical equilibria to maintain constant low supersaturations, which realized a significant improvement over previously reported syntheses. Axial screw dislocations, whose presence are confirmed by both diffraction contrast TEM images and twist contour analysis, enable the 1D growth of NWs observed. We note that, unlike previous reports where either surfactants or organic ligands are used and argued to be important in the NW synthesis, our synthetic method requires only the simple inorganic precursors Fe^{2+} and Fe. By controlling the hydrolysis of Fe^{3+} and therefore the supersaturation level of Fe^{3+}, conditions that favor dislocation-driven crystal growth are created, enabling more effective α-FeOOH NW growth. It would be interesting if the roles of surfactants or organic ligands could be examined from the viewpoint of controlling supersaturation in the solution system, as many are multidentate ligands or pH buffers. The as-synthesized α-FeOOH NWs can be readily converted into single-crystal porous α-Fe_2O_3 NWs, which have potential applications in solar energy conversion. These results support the generality of dislocation-driven nanomaterial growth and show that, with new understanding and proper design on how to control the supersaturation, many more useful materials can be grown into 1D morphologies via the dislocation-driven mechanism in aqueous solutions at low cost.

■ ASSOCIATED CONTENT

Supporting Information. Details of experimental procedures, discussion on bend contour analysis, additional TEM figures, and PXRD of static reaction products. This material is available free of charge via the Internet at http://pubs.acs.org.

■ AUTHOR INFORMATION

Corresponding Author
jin@chem.wisc.edu

■ ACKNOWLEDGMENT

This research is supported by NSF (CAREER DMR-0548232). S.J. also thanks Sloan Research Fellowship for support. S.A.M. was partially supported by a 3M Graduate Research Fellowship and by UW-Madison NSEC (NSF DMR 0832760).

■ REFERENCES

(1) (a) Bierman, M. J.; Lau, Y. K. A.; Kvit, A. V.; Schmitt, A. L.; Jin, S. *Science* **2008**, *320*, 1060–1063. (b) Lau, Y. K. A.; Chernak, D. J.; Bierman, M. J.; Jin, S. *J. Am. Chem. Soc.* **2009**, *131*, 16461–16471. (c) Morin, S. A.; Bierman, M. J.; Tong, J.; Jin, S. *Science* **2010**, *328*, 476–480. (d) Morin, S. A.; Jin, S. *Nano Lett.* **2010**, *10*, 3459–3463. (e) Sears, G. W. *Acta Met.* **1955**, *3*, 367–369. (f) Jin, S.; Bierman, M. J.; Morin, S. A. *J. Phys. Chem. Lett.* **2010**, *1*, 1472–1480.

(2) (a) Wagner, R. S.; Ellis, W. C. *Appl. Phys. Lett.* **1964**, *4*, 89–90. (b) Morales, A. M.; Lieber, C. M. *Science* **1998**, *279*, 208–211. (c) Xia, Y.; Yang, P.; Sun, Y.; Wu, Y.; Mayers, B.; Gates, B.; Yin, Y.; Kim, F.; Yan, H. *Adv. Mater.* **2003**, *15*, 353–389.

(3) Zhu, J.; Peng, H. L.; Marshall, A. F.; Barnett, D. M.; Nix, W. D.; Cui, Y. *Nat. Nanotechnol.* **2008**, *3*, 477–481.

(4) Li, Y.; Wu, Y. *Chem. Mater.* **2010**, *22*, 5537–5542.

(5) (a) Jacobs, B. W.; Crimp, M. A.; McElroy, K.; Ayres, V. M. *Nano Lett.* **2008**, *8*, 4353–4358. (b) Cherns, D.; Meshi, L.; Griffiths, I.; Khongphetsak, S.; Novikov, S. V.; Farley, N. R. S.; Campion, R. P.; Foxon, C. T. *Appl. Phys. Lett.* **2008**, *93*, 111911.

(6) (a) Kennedy, J. H.; Frese, K. W. *J. Electrochem. Soc.* **1978**, *125*, 709–714. (b) Sanchez, C.; Sieber, K. D.; Somorjai, G. A. *J. Electroanal. Chem.* **1988**, *252*, 269–290.

(7) (a) Kay, A.; Cesar, I.; Gratzel, M. *J. Am. Chem. Soc.* **2006**, *128*, 15714–15721. (b) van de Krol, R.; Liang, Y. Q.; Schoonman, J. *J. Mater. Chem.* **2008**, *18*, 2311–2320. (c) Brillet, J.; Gratzel, M.; Sivula, K. *Nano Lett.* **2010**, *10*, 4155–4160.

(8) (a) Ozaki, M.; Kratohvil, S.; Matijevic, E. *J. Colloid Interface Sci.* **1984**, *102*, 146–151. (b) Saric, A.; Music, S.; Nomura, K.; Popovic, S. *Mater. Sci. Eng. B—Solid* **1998**, *56*, 43–52. (c) Beermann, N.; Vayssieres, L.; Lindquist, S. E.; Hagfeldt, A. *J. Electrochem. Soc.* **2000**, *147*, 2456–2461. (d) Vayssieres, L.; Beermann, N.; Lindquist, S. E.; Hagfeldt, A. *Chem. Mater.* **2001**, *13*, 233–235. (e) Xiong, Y.; Xie, Y.; Chen, S. W.; Li, Z. Q. *Chem.—Eur. J.* **2003**, *9*, 4991–4996. (f) Tang, B.; Wang, G. L.; Zhuo, L. H.; Ge, J. C.; Cui, L. J. *Inorg. Chem.* **2006**, *45*, 5196–5200. (g) Liu, L.; Kou, H. Z.; Mo, W. L.; Liu, H. J.; Wang, Y. Q. *J. Phys. Chem. B* **2006**, *110*, 15218–15223. (h) Fang, X. L.; Chen, C.; Jin, M. S.; Kuang, Q.; Xie, Z. X.; Xie, S. Y.; Huang, R. B.; Zheng, L. S. *J. Mater. Chem.* **2009**, *19*, 6154–6160.

(9) Markov, I. V. *Crystal Growth For Beginners: Fundamentals of Nucleation, Crystal Growth, and Epitaxy*, 1st ed.; World Scientific Publishing Co. Pte. Ltd.: Singapore, 1995.

(10) Navrotsky, A.; Mazeina, L.; Majzlan, J. *Science* **2008**, *319*, 1635–1638.

(11) Eshelby, J. D. *J. Appl. Phys.* **1953**, *24*, 176–179.

(12) Drum, C. M. *J. Appl. Phys.* **1965**, *36*, 824–829.

(13) Cudennec, Y.; Lecerf, A. *Solid State Sci.* **2005**, *7*, 520–529.

(14) (a) Li, Y. G.; Tan, B.; Wu, Y. Y. *J. Am. Chem. Soc.* **2006**, *128*, 14258–14259. (b) Li, Y. G.; Tan, B.; Wu, Y. Y. *Chem. Mater.* **2008**, *20*, 2602–2602. (c) Tian, Z. R.; Tong, W.; Wang, J. Y.; Duan, N. G.; Krishnan, V. V.; Suib, S. L. *Science* **1997**, *276*, 926–930. (d) Zhang, X. J.; Shi, W. H.; Zhu, J. X.; Zhao, W. Y.; Ma, J.; Mhaisalkar, S.; Maria, T. L.; Yang, Y. H.; Zhang, H.; Hng, H. H.; Yan, Q. Y. *Nano Res.* **2010**, *3*, 643–652.